



## Towards timing and stratigraphy of the Bronze Age burial mound royal tomb (Königsgrab) of Seddin (Brandenburg, northeastern Germany)

Moritz Nykamp<sup>1</sup>, Jacob Hardt<sup>1</sup>, Philipp Hoelzmann<sup>1</sup>, Jens May<sup>2</sup>, and Tony Reimann<sup>3,4</sup>

<sup>1</sup>Institute of Geographical Sciences, Freie Universität Berlin, Berlin, Germany

<sup>2</sup>Brandenburgisches Landesamt für Denkmalpflege und Archäologisches Landesmuseum, OT Wünsdorf, Zossen, Germany

<sup>3</sup>Soil Geography and Landscape group & Netherlands Centre for Luminescence dating, Wageningen University, Wageningen, the Netherlands

<sup>4</sup>Institute of Geography, University of Cologne, Cologne, Germany

**Correspondence:** Moritz Nykamp ([m.nykamp@fu-berlin.de](mailto:m.nykamp@fu-berlin.de))

**Relevant dates:** Received: 15 April 2020 – Revised: 13 November 2020 – Accepted: 26 November 2020 – Published: 12 January 2021

**How to cite:** Nykamp, M., Hardt, J., Hoelzmann, P., May, J., and Reimann, T.: Towards timing and stratigraphy of the Bronze Age burial mound royal tomb (Königsgrab) of Seddin (Brandenburg, northeastern Germany), *E&G Quaternary Sci. J.*, 70, 1–17, <https://doi.org/10.5194/egqsj-70-1-2021>, 2021.

**Abstract:** This study uses an integrated multi-method geoarcheological and geochronological approach to contribute to the understanding of the timing and stratigraphy of the monumental burial mound royal tomb (Königsgrab) of Seddin. We show that the hitherto established radiocarbon-based terminus post quem time frame for the construction of the burial mound of 910–800 BCE is supported by optically stimulated luminescence (OSL) dating. The radiocarbon samples were obtained from a substrate directly underneath the burial mound which supposedly represents the late glacial/Holocene soil that was buried below the structure. We use sedimentological (grain-size analyses) and geochemical analyses (element analyses, carbon, pH, and electric conductivity determinations) to reassess and confirm this hypothesis. In addition to the burial age associated with the last anthropogenic reworking during construction of the burial mound, the OSL dating results provide new insights into the primary deposition history of the original substrates used for the structure. In combination with regional information about the middle and late Quaternary development of the environment, our data allow us to provide a synoptic genetic model of the landscape development and the multiphase stratigraphy of the royal tomb of Seddin within the Late Bronze Age cultural group “Seddiner Gruppe” of northern Germany. Based on our initial experiences with OSL dating applied to the sediments of a burial mound – to the best of our knowledge the first attempt in Europe – we propose a minimal invasive approach to obtain datable material from burial mounds and discuss related opportunities and challenges.

**Kurzfassung:** Diese Studie nutzt einen integrativen geoarchäologisch-geochronologischen Ansatz, um einen Beitrag zum Verständnis der Chronologie und Stratigraphie des monumentalen Grabhügels „Königsgrab“ von Seddin zu leisten. Wir zeigen, dass der bislang etablierte, auf Radiokarbonaten basierende, post quem Zeitrahmen von 910–800 BCE für die Errichtung des Grabhügels durch optisch-stimulierte Lumineszenz (OSL) Alter unterstützt wird. Die Proben für die Radiokarbonatierung stammen aus

einem Substrat unterhalb des Grabhügels, das den vermeintlich begrabenen spätglazialen/holozänen Boden repräsentiert. Wir nutzen sedimentologische (Korngrößenanalysen) und geochemische Analysen (Elementaranalyse, Kohlenstoffbestimmung, pH- und elektrische Leitfähigkeitsmessung), um diese Annahme zu evaluieren und zu bestätigen. Ergänzend zu dem Alter der Überdeckung des spätglazialen/holozänen Bodens, das mit der letzten anthropogenen Materialumlagerung während der Konstruktion des Grabhügels assoziiert wird, geben die Ergebnisse der OSL-Datierungen einen Einblick in die ursprüngliche Ablagerungsgeschichte des Ausgangssubstrates, das für die Errichtung des Grabhügels verwendet wurde. In Kombination mit Informationen zur regionalen mittel- bis spätquartären Landschaftsentstehung, lässt sich aus unseren Daten ein genetisches Übersichtsmodell der Landschaftsentwicklung und der mehrphasigen Stratigraphie des „Königsgrabes“ von Seddin als Teil der spätbronzezeitlichen Kulturgruppe „Seddiner Gruppe“ von Norddeutschland ableiten. Auf Grundlage unserer ersten Erfahrungen mit der OSL-Datierung von Sedimenten eines Grabhügels, nach unserem Wissen der erste Versuch in Europa, schlagen wir einen minimalinvasiven Ansatz vor, um datierbares Material aus Grabhügeln zu gewinnen und diskutieren damit verbundene Möglichkeiten und Herausforderungen.

## 1 Introduction

Burial mounds form part of the most important monuments of European prehistory, and many thousands of these architectural elements are still visible in the landscapes of Europe (Doorenbosch, 2013). Furthermore, new technologies such as high-resolution lidar-derived digital elevation models that are more and more available will likely increase the number of newly discovered monuments significantly.

Generally, burial mounds are an important form of burial practice as they serve as a permanent marker of a dead person, keeping them in the memory of those who live on (Harding, 2012). In northern Central Europe, they occur from the Neolithic to the Slavic period/Viking age.

Although archeologists from the different European regions and specialists for certain cultural epochs are usually able to date newly discovered burial mounds based on their external appearance, numerical age control is often still required to reliably relate a burial mound to a specific cultural epoch. This mostly requires excavation for either archeological artifacts or macroscopic remains of organic matter suitable for  $^{14}\text{C}$  dating – the former is undesirable in many cases for the purposes of cultural heritage preservation and the latter is often difficult to obtain (Kristiansen et al., 2003). Kristiansen et al. (2003), therefore, propose an approach with minimal disturbance to obtain samples for  $^{14}\text{C}$  analysis of soil organic matter fractions. They demonstrate that augering through the mound can provide suitable samples from former surface soils buried by the mound and that  $^{14}\text{C}$  dating of soil organic matter fractions can yield good results. Their results show that the humic acid fractions in 7 out of 10 mounds are in good agreement with the reference ages (Kristiansen et al., 2003). Relying on the presence of a buried organic-rich topsoil horizon alone can, however, be problematic: it might be lacking as a consequence of soil erosion after vegetation clearance or surface leveling prior to the construction

of the mound. Sand-sized quartz grains suitable for optically stimulated luminescence (OSL) dating, in contrast, can be regarded as ubiquitous in most (if not all) burial mounds located along the European sand belt. However, to the best of our knowledge, OSL dating has not yet been performed on burial mounds in Europe, unlike examples from archeological mound structures (e.g., tells and burial mounds) in the USA, Israel, and Jordan (e.g., Feathers, 1997; Porat et al., 2012; Pluckhahn et al., 2015; al Khasawneh et al., 2020).

A precisely dated burial mound and thus an ideal test object for OSL dating of mound sediments is the royal tomb (Königsgrab) of Seddin (federal state of Brandenburg, northeastern Germany). It dates to the 9th century BCE and is considered one of the most important tombs of the Nordic Bronze Age and an excellent example of an elite or chief tomb (May, 2018). The mound was piled up in layers consisting of alternating strata of erratic boulders and sand (May and Hauptmann, 2012; May, 2018). A stone pavement followed by a sand layer form the lowermost layers. The construction continues with a second stone pavement and another sand layer. A third stone pavement forms the uppermost deposit. During archeological excavations, at several locations a layer of either dark substrate or pale solidified sand was identified directly underneath the basal stone pavement, i.e., in stratigraphically identical positions. The dark material was interpreted as a paleosol that was buried during the initial construction phase by the boulders of the first stone pavement (May, 2018). However, geoscientific analyses to support the interpretation of a buried paleosol underneath the royal tomb including the pedological horizon designation of the dark substrate and the pale sand are currently lacking. The additional information can provide important insights into the conditions and processes immediately preceding the initial construction phase of the burial mound, e.g., potential erosion by water or wind of the organic-rich topsoil horizon after vegetation clearance or possible leveling of the founda-

tion soil. The pedological characterization of the buried soil horizons also helps to assess their potential for additional paleoenvironmental studies such as pollen analyses from fossil organic-rich topsoil horizons (e.g., Kaiser et al., 2020).

Radiocarbon ages obtained from pieces of charred wood from the dark layer provide a rather precise terminus post quem time frame for the construction of the burial mound ranging from 910 to 800 BCE (May and Hauptmann, 2012; May, 2018). These ages provide a maximum age estimate for the construction of the burial mound but are completely decoupled from the construction process (cf. Pluckhahn et al., 2015). Thus, even though the age range is precise, independent numerical age control obtained by a dating technique that is capable of recording the construction process itself such as OSL dating is useful.

Therefore, the aims of this contribution are to provide (i) independent numerical age estimates to verify the terminus post quem time frame of the construction period by applying OSL dating to capture the construction process and (ii) sedimentological and geochemical analyses to further investigate and classify the suggested buried paleosol.

We present a compilation of radiocarbon and OSL ages and thereby contribute to the chronology of the royal tomb of Seddin by applying two dating methods that are independent of each other. Moreover, our OSL datings also provide important insights into the Quaternary history of the construction material itself. We combine the local chronological and sediment/soil data with regional information on the middle and late Quaternary environmental history to set up a genetic model of the landscape development and possible construction phases of the royal tomb of Seddin. Furthermore, we discuss opportunities and challenges of a minimally invasive approach – following Kristiansen et al. (2003) – in combination with luminescence dating techniques to provide initial numerical age estimates for newly discovered burial mounds.

## 2 Regional setting and archeological background

### 2.1 Regional setting

The royal tomb (Königsgrab) of Seddin is located in the Prignitz region approximately 2 km southwest of the village of Seddin, in the northwest of the federal state of Brandenburg, northeast Germany (Fig. 1).

The monumental burial mound is situated in the middle reaches of the Stepenitz river, a smaller lowland tributary of the Elbe river discharging into the North Sea. The area is part of the old morainic glacial landscape that was initially formed by the Scandinavian Ice Sheet (SIS) during the penultimate Saalian glaciation (~ late MIS 6, marine isotope stage; Ehlers et al., 2011; Lippstreu et al., 2015) and afterwards altered by periglacial processes during the last Weichselian ice age (mainly MIS 4 and MIS 2).

The late Saalian deposits in the vicinity of the burial mound comprise till, as well as glaciofluvial sand and gravel

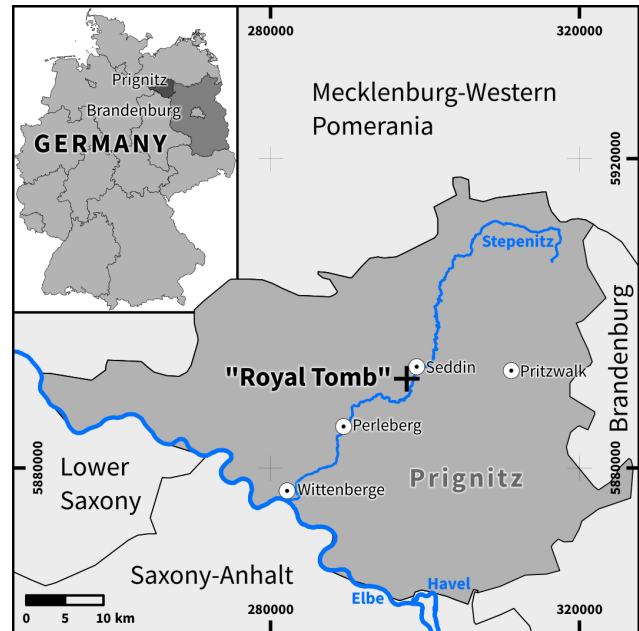


**Figure 1.** Overview map showing the Prignitz region in north-west Brandenburg (northeast Germany) and the location of the royal tomb of Seddin (reference system: WGS84; projection: UTM33N; data sources: Naturalearthdata, 2020; Offenedaten, 2020; Geofabrik, 2020).

(Fig. 2a). The smoothly undulating topography of the area is a result of periglacial reworking processes, e.g., gelifluction, and coversand formation. This landscape type is characterized as old morainic landscape (Lippstreu et al., 1997; Nagel et al., 2003; Lippstreu et al., 2015). Direct numerical ages of the late Saalian sediments are generally rare in the region and are lacking for the wider surroundings of the burial mound. OSL ages of Saalian glaciofluvial deposits from the south of Brandenburg (Beelitz, ca. 120 km southeast of Seddin) yielded an age range of 150–130 kyr (Lüthgens et al., 2010). This is in agreement with previous age estimates that were based on stratigraphic and morphostratigraphic correlations (Litt et al., 2007; Böse et al., 2012). Coversand formation probably took place starting at the end of the Weichselian Pleniglacial, as was shown at different sites within the European sand belt (Kasse, 2002; Koster, 2005; Kaiser et al., 2009). Coversands at Beelitz were dated to ~ 15 ka by means of OSL (Lüthgens et al., 2010).

“Fahlerde” or “Braunerde-Fahlerde” (according to Ad-Hoc-AG Boden, 2005, and MLUV, 2005), i.e., Luvisols (according to IUSS Working Group WRB, 2006), have developed in the sandy to loamy-sandy substrates (Fig. 2). These soils form one of the typical soils in the Prignitz region (MLUV, 2005; GeoBasis-DE/LGB, 2012) and are predominant in the surroundings of the royal tomb (Fig. 2b).

The onset of soil formation in the region was in the Late Glacial, as shown by micromorphological analyses (Kühn,

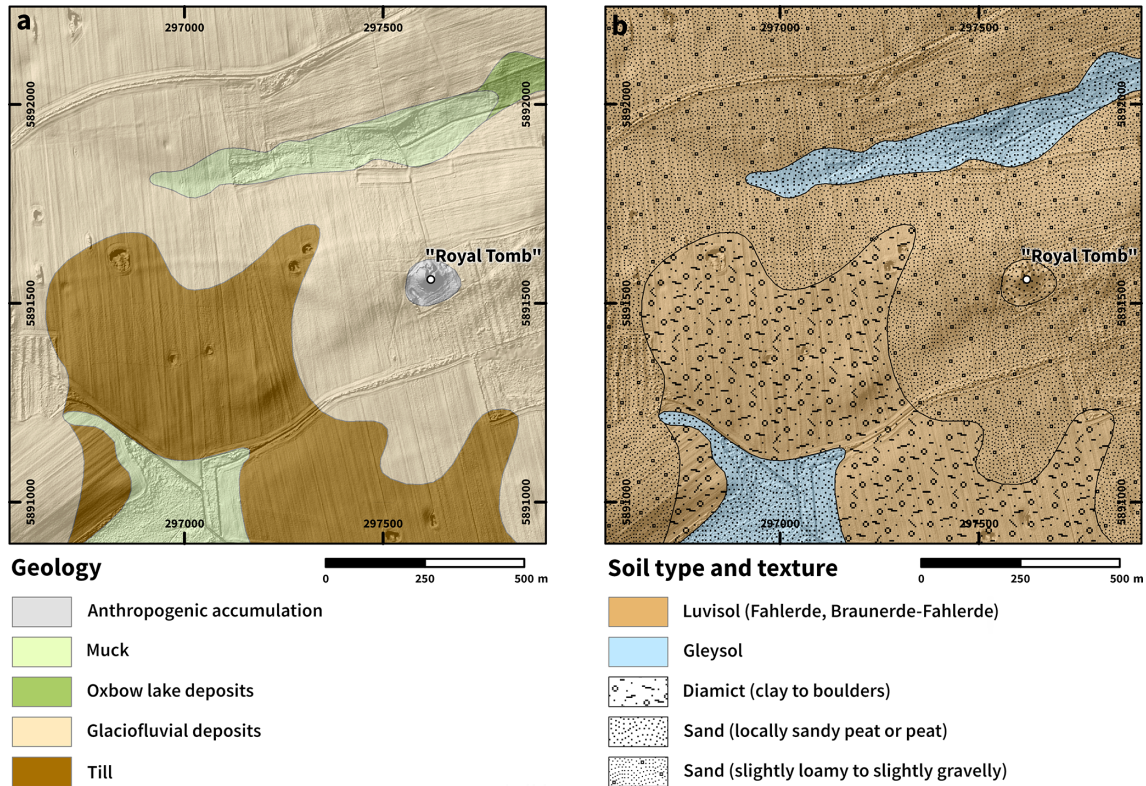


**Figure 2.** Simplified overview maps showing (a) the geology and (b) the dominating soil types and textures in the surroundings of the royal tomb (reference system: WGS84; projection: UTM33N; data sources: Schulte and Wahnschaffe, 1905; GeoBasis-DE/LGB, 2012; LBGR Brandenburg, 2020).

2003) and a review of available geochronological data on soil formation in northeast Germany (Kappler et al., 2019).

Palynological evidence from different archives in Brandenburg show a simultaneous increase in human activity in the Late Bronze Age compared to the Early and Middle Bronze Age. Increasing frequencies of cereal-type pollen and secondary anthropogenic indicators document the strong human impact on the vegetation; strongly decreasing arboreal pollen points to large-scale clearings of woodland (Jahns, 2015, 2018). The pollen diagram from the Bergsoll, i.e., a small wetland area ca. 7.2 km northeast of the royal tomb, provides evidence for extensive deforestation in ca. 800 BCE (Jahns, 2018). Also, a distinct decline of *Quercus* pollen at the Sacrower See lake in ca. 800 BCE suggests the intensive use of oak lumber that resulted in a shift of the forest composition (Jahns, 2015). These results from archives in Brandenburg are in agreement with results of pollen and charcoal analyses from fossil soils in south Mecklenburg-Western Pomerania indicating the first human impacts on the vegetation during the Neolithic and an intensification during the Bronze Age; fire events started to increase roughly around the transition from the Bronze Age to the Iron Age (Kaiser et al., 2020). The present-day land cover in the surroundings

of the royal tomb is dominated by arable land, pastures, and forests (European Environment Agency, 2020).

The study site is located at the transition from a temperate oceanic climate in the west to a humid continental climate in the east (i.e., west–east transition from Cfb to Dfb according to the Köppen–Geiger classification; Beck et al., 2018). The weather station Marnitz (German Meteorological Service, DWD; station ID: 3196) is located ca. 20 km north of the study area at an elevation of 81.0 m above sea level. This station recorded a mean annual air temperature of 8.2 °C (range: 7.1–9.9 °C) and a mean annual precipitation of 660 mm a<sup>-1</sup> (range: 460–816 mm a<sup>-1</sup>) for the period 1961–1990 (DWD Climate Data Center, 2020a, b).

## 2.2 Archeological background

The locality of the royal tomb of Seddin was eponymous for the cultural group “Seddiner Gruppe” in southwest Mecklenburg and northwest Brandenburg (May and Hauptmann, 2012) in the Late Bronze Age (1100 to 530 BCE). It is considered one of the most important tombs of the 9th century BCE in northern Central Europe and an excellent example of an elite or chief tomb at the transition from the Late Bronze Age to the Iron Age (May and Hauptmann, 2012). Its isolated position, as well as the presence of other richly equipped

graves in the area, indicates the existence of an elite during the Late Bronze Age at the southern margin of the Nordic Bronze Age cultural groups (May, 2018).

The burial mound has a diameter of ca. 61.5 m, and its original height was ca. 9 m. Erratic boulders form a circle around the foot of the grave mound. This circle has a circumference of ca. 193.5 m surrounding an area of ca. 3000 m<sup>2</sup> (May, 2018). It is likely that the stone ring was built before the mound was erected. The mound itself was built of alternating strata of stones and sand, and it was piled up in layers. Due to its monumental dimensions it was visible from all directions over several kilometers, at least during periods of sparse vegetation (May, 2018). Palynological analyses at the Bergsoll near Seddin point to widespread deforestation in the area during the Bronze Age, and thereby it seems likely that the burial mound represented a landmark at this time (Jahns, 2018). In combination with the surrounding grave mounds and grave mound fields, it exemplifies the ritual use and re-organization of the area (May, 2018).

A large burial chamber made of stones is located inside the mound. This chamber is situated ca. 9 m to the southeast of the center of the stone circle and was built on level ground (May, 2018). The chamber contained painted clay plasters and rich burial equipment consisting of 41 objects and the cremated remains of three individuals. A 30–40-year-old man was buried together with two presumably younger women (Kiekebusch, 1928; May and Hauptmann, 2005, 2011).

The royal tomb of Seddin was initially dated based on the archeological findings from the burial chamber. Researchers agree that the youngest objects of the burial equipment date to period V based on Montelius (1885). Period V is, according to Montelius (1885), one out of six (I–VI) relative chronological periods for the Nordic Bronze Age. Stratigraphy, typology, and coincident findings (*geschlossene Funde*), such as all objects obtained from a grave or hoard for which a coincident laying down is assumed, form the basis for the relative chronological periodization of the archeological findings. Therefore, the exact timing and duration of the periods is controversial among archeologists. In the case of the royal tomb of Seddin, it is agreed upon that the burials belong to Montelius' period V, but there is no consensus regarding its placement within this period. While Wüstemann (1974) dates the burial equipment to an early phase of period V, Kossinna (1910) argues that the equipment rather points to a late phase of period V, i.e., dating to ca. 800 BCE. Thus, both ends of the temporal assignment of the burial equipment within period V are covered by these opinions. Owing to numerical dating techniques, e.g., radiocarbon dating, the timing and duration of the periods become more precise. One of the most recent advances in providing accurate numerical dates of coincident findings is the radiocarbon dating of cremated human remains. Such an example is provided by Hornstrup et al. (2012) who radiocarbon dated cremated hu-

man remains from Danish graves and thereby suggest that period V covers the time span from 950/920 to 800 BCE.

In the course of archeological investigations, four radiocarbon dates were obtained from charcoal fragments recovered from four different trenches in close proximity to the inner side of the stone ring of the burial mound of Seddin (Fig. 3). Each of these radiocarbon samples originates from a substrate which most likely corresponds to layer 3 of profile SD17P1 (Fig. 4). Three of the obtained charcoal pieces were dated to 910–800 BCE (at  $2\sigma$  range; Table 2). This agrees well with the abovementioned estimation of the duration of period V. These ages also provide a terminus post quem for the construction of the burial mound since the construction of the burial mound rests directly on layer 3 (Fig. 4). The fourth radiocarbon sample (MAMS 35030; Fig. 3) was obtained from a stratigraphic position that is identical with layer 3 of profile SD17P1 (Fig. 4). However, while layer 3 of profile SD17P1 consists of dark organic-rich material (see below), sample MAMS 35030 (*Fagus* charcoal) was taken from a layer consisting of white, strongly solidified sand and is dated to 1740–1620 BCE (at  $2\sigma$  range; Table 2). This age is roughly 790 years older than the oldest dating of the grave. At the current state of research, it remains unclear whether this indicates a previous use of the area where the burial mound was erected later on or if the sample is affected by the “old wood effect” as is the case for other radiocarbon samples obtained from locations close by (May, 2018).

### 3 Material and methods

#### 3.1 Field work

Profile SD17P1 (5891584 N, 297601 E; UTM 33N) was recorded in August 2017 during archeological excavations on the northwestern slope of the Bronze Age burial mound (Fig. 3). The profile was excavated in three ca. 1 m deep sections separated by ca. 1 m wide steps. It was cleaned and documented by photographs (Fig. 4a) before the sediment succession was described and sampled. The macroscopic sediment description was carried out according to the German manual for soil mapping (KA 5; Ad-Hoc-AG Boden, 2005) and includes texture, humus content, redoximorphic features, layer boundaries, and signs of pedogenic processes. The English terminology follows Schoeneberger et al. (2012). Colors were recorded using the Munsell soil color charts and converted to RGB values to allow realistic colorization of the profile drawing. A total of 39 sediment samples were extracted for more detailed particle size and geochemical analyses (Sect. 3.2). Additionally, three samples for luminescence dating and bulk samples for gamma spectrometry measurements were obtained; OSL samples were extracted with metal tubes (25 cm length,  $\varnothing$  5 cm) that were covered with aluminum foil and plastic caps (Sect. 3.3).

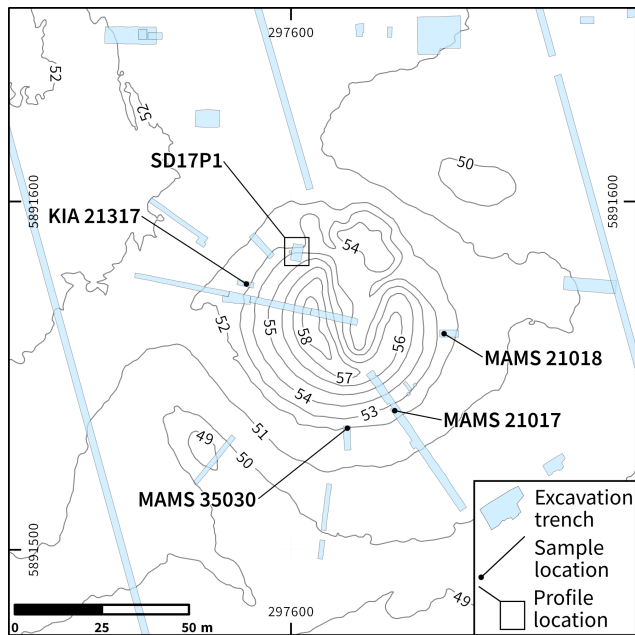


**Figure 3.** Topographic plan of the close vicinity of the royal tomb of Seddin (in the center) showing the locations of the excavation trenches, the radiocarbon-dated charcoal fragments (Table 2), and profile SD17P1 (reference system: WGS84; projection: UTM33N; contour lines were derived from lidar-based 1 m elevation data; GeoBasis-DE/LGB, 2020).

### 3.2 Sediment analyses

Sediment analyses comprise particle size analyses, pH, electric conductivity, and total carbon (TC) measurements, and Fe, Al, and Si determinations to characterize the sediments and to identify potential paleosurfaces within the profile. Sample preparation included drying at 105 °C in a drying cabinet, crushing aggregates, separation of coarse components with a 2 mm sieve, and homogenizing the <2 mm sub-samples in a vibrating disk mill for carbon and p-ED-XRF (portable energy-dispersive X-ray fluorescence) analyses.

The grain size distributions were determined for the fraction  $\leq 1$  mm using a laser diffraction particle size analyzer; particle size classes are defined according to Ad-Hoc-AG Boden (2005).

Total carbon (TC) contents were determined using a CHN analyzer. All samples were tested negatively for inorganic carbon using 10 % HCl and therefore the TC contents are regarded as presenting total organic carbon (TOC) contents.

A wide range of chemical elements were measured with a portable energy-dispersive X-ray fluorescence spectrometer. Selected elements (Al, Si, Fe) are used after quality control to characterize the sediments of the burial mound.

Further details on analytical steps and quality control are included in the Supplement.

### 3.3 OSL dating

OSL dating was used to determine the time of burial of three sand-sized quartz samples from profile SD17P1. The analyses were carried out at the Netherlands Centre for Luminescence dating at Wageningen University. To calculate an OSL age, two quantities need to be measured: (i) the paleodose (in Gy), which is the amount of dose that was received by the sample since it was last exposed to sunlight, and (ii) the amount of ionizing radiation that the sample is exposed to during burial, which is termed the dose rate (in  $\text{Gy kyr}^{-1}$ ).

Purified quartz-rich extracts of 212–250  $\mu\text{m}$  grain size were used for paleodose determination. For equivalent dose measurements, the SAR protocol of Murray and Wintle (2003) was applied to small 1 mm aliquots ( $\sim 15$ –50 grains per aliquot). The most light-sensitive OSL signal of quartz grains is selected using the early background approach (Cunningham and Wallinga, 2010). The performance and heat treatment of this protocol was tested by dedicated dose recovery experiments. The most optimal dose recovery ratio ( $1.01 \pm 0.05$ ,  $n = 13$ ) was obtained with a combination of 220, 200, and 230 °C for preheat, cut-heat, and hot-bleach, respectively. To obtain meaningful single-aliquot equivalent dose ( $D_e$ ) distributions, we measured 96 aliquots per sample with around 50 % of the aliquots providing a sufficient OSL signal. The  $D_e$  distributions derived from the acceptable single-aliquot  $D_e$  values revealed significantly more scatter than we would expect for a well-bleached and unmixed sample. To obtain the paleodose that can be associated with the youngest single-aliquot population, the bootstrap version of the minimum age model (bootMAM; Galbraith et al., 1999; Cunningham et al., 2012) was applied. This model was run with a sigma\_b input parameter of  $15 \pm 5$  % (van der Meij et al., 2019).

To obtain the activity concentration associated with the decay of  $^{40}\text{K}$  and the uranium and thorium decay chains, we performed high-resolution gamma spectrometry measurements on dry bulk sediment samples. Activity concentrations were converted to beta and gamma dose rates using the conversion factors of Guérin et al. (2011). Grain size, water, and organic matter attenuation effects were incorporated using the equations provided by Mejdahl (1979) and Aitken (1985). The moisture content of the sample's surroundings was estimated to be  $6 \pm 3$  %, associated with relatively well-sorted and well-drained sandy deposits. The corresponding cosmic dose rate of a sample was calculated according to Prescott and Hutton (1994).

## 4 Results

### 4.1 Sediment description

The recorded profile SD17P1 reaches a total depth of 314 cm below the present-day surface of the burial mound and consists of 25 macroscopically distinguishable layers (Fig. 4).

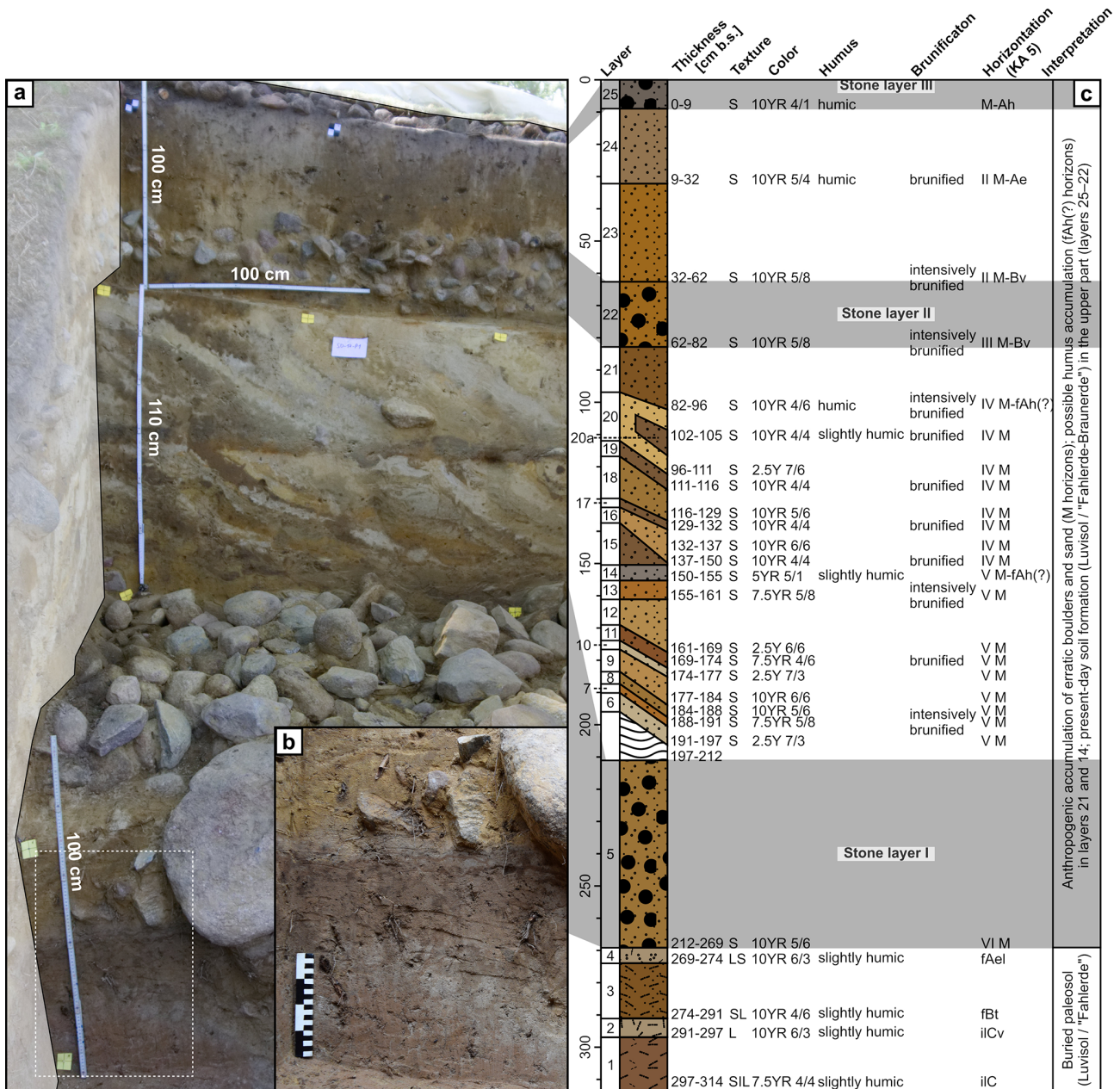


**Figure 4.** Composite illustration of (a) photograph of profile SD17P1 after cleaning (the white box in a marks the approximate extent of b); (b) detailed photograph of the lowest part of the profile; and (c) schematic drawing according to the field description, including summarized sediment characteristics (texture: S is sand, LS is loamy sand, SL is sandy loam, L is loam, SIL is silty loam) and pedological horizon designation according to KA 5 (Ad-Hoc-AG Boden, 2005). Designation of soil horizons includes the naming of the horizons (A is topsoil horizon, B is subsoil horizon, C is parent material, M is anthropogenic accumulation; prefixes: f is fossil, i is siliceous, l is loose; suffixes: e is leached-out, h is humus rich, l is depleted in clay, t is enriched in clay, v is weathered, brunified) and the counting of the main sand and stone strata (roman numerals are main strata of the anthropogenic accumulation). The gray shaded areas in (c) represent the three stone layers that structure the profile. For reference to the texture symbology, see Fig. 5.

The section is characterized by three artificial stone layers at 0–9, 62–82, and 212–269 cm b.s. (below surface) that consist of glacial boulders with up to 80 cm edge length. According to May (2018), the three stone layers are numbered I to III from the bottom to the top. The indication below surface refers to the surface of the burial mound at the location of the excavation trench, and the layers are counted from 1 to 25 (including the stone layers) from bottom to top. Between the stone layers, loose, sandy material was deposited during the construction of the burial mound (May, 2018). The upper 21 layers, between 0 and 269 cm b.s., represent material that was piled up during the construction of the burial mound.

Layer 25 (0–9 cm b.s.) represents the uppermost stone layer (III) that covers the burial mound. The stones are embedded in a dark gray (10YR 4/1) humic matrix consisting of sand. Layers 24 (9–32 cm b.s.) and 23 (32–62 cm b.s.) between stone layer III and II consist of sand and show gradual to diffuse layer boundaries. The color is yellowish brown with an increasing chroma towards the bottom (layer 24 is 10YR5/4; layer 23 is 10YR 5/8). The humus content decreases with depth, while brunification increases. Layer 22 (62–82 cm b.s.) represents stone layer II. The stones are embedded in brunified, yellowish brown (10YR 5/8) sand. Between stone layer II and stone layer I (82–212 cm b.s.), two packages of inclined layers (layers 21–15 and layers 12–6) are present. These two packages are separated by two horizontally running layers (layers 14 and 13). The inclined and the horizontal layers between stone layers II and I consist of sand, show varying humus contents and brunification intensities, and mostly have clearly defined layer boundaries. Layer 5 (212–269 cm b.s.) represents stone layer I. The stones, mostly cobble to stone size and partly up to boulder size, are embedded in slightly brunified yellowish brown (10YR 5/6) sand.

Layer 4 (269–274 cm b.s.) consists of pale brown (10YR 6/3) loamy sand with occasional fine gravels and horizontal dark yellowish brown (10YR 3/4) bands; the boundaries with layers 5 and 3 are abrupt. Layer 3 (274–291 cm b.s.) is characterized by dark yellowish brown (10YR 4/6), slightly mottled sandy loam and shows a clear to gradual wavy boundary with layer 2 (291–297 cm b.s.), which consists of pale brown (10YR 6/3) loam. The boundary of layers 2 and 1 is gradual and wavy, and the lowermost layer 1 (297–314 cm b.s.) is composed of brown (7.5YR 4/4) silt loam.

Based on this detailed description, profile SD17P1 is subdivided into the base representing the remnants of a buried paleosol developed from glaciofluvial loamy sand (layers 4 and 3) above till (layers 2 and 1) and alternating layers of anthropogenically heaped up stones and sand (layers 5–25) forming the upper part of the sequence (Fig. 4c).

#### 4.2 Grain size distributions and geochemical characteristics

The grain size distributions of the upper 21 layers are rather uniform, ranging between 79.6 vol % and 98.5 vol % sand ( $\bar{x} = 90.9$  vol %;  $\sigma = 5.1$  vol %;  $n = 34$ ) with only minor silt and clay contents (Fig. 5). In these sediments, medium sand is the major grain size fraction. The material below becomes increasingly fine. Layers 4 and 3 show decreasing sand ( $\bar{x} = 69.7$  vol %;  $\sigma = 8.4$  vol %;  $n = 3$ ) and increasing silt and clay contents. The loamy material of the two lowermost sections (2 and 1) show the lowest sand ( $\bar{x} = 36.9$  vol %;  $\sigma = 4.6$  vol %;  $n = 2$ ) and the highest silt and clay contents.

The sediments of layer 25 (0–9 cm b.s.) show the highest concentration of total carbon (TC = 2.14 mass %), intermediate electrical conductivity (EC = 71  $\mu\text{S cm}^{-1}$ ) values, and strong acidity (pH = 3.2). With depth, the TC and EC concentrations decrease towards the bottom of layer 22 (62–82 cm b.s.; TC = 0.23 mass %; EC = 24  $\mu\text{S cm}^{-1}$ ), while the pH values markedly increase to 4.5. At the top of layer 21 (82–96 cm b.s.), the TC concentrations (0.82 mass %) and, to a lesser extent, the EC values (52  $\mu\text{S cm}^{-1}$ ) increase abruptly, and the pH values show a slight decrease to 4.3. Between 96 and 150 cm depth (layers 20–15), the TC concentrations and the EC values show little variation; the pH values vary slightly more. The sediments of layers 14 (150–155 cm b.s.) and 13 (155–161 cm b.s.) show slightly increased TC concentrations ( $\bar{x} = 0.44$  mass %) compared to the layers above and below. The EC shows a strong increase in layer 13 (111  $\mu\text{S cm}^{-1}$ ), whereas the pH value decreases to 3.8. Between layers 12 (161–169 cm b.s.) and 5 (212–269 cm b.s.), the TC contents slightly vary in the lower range of values; the EC values slightly decrease and then slightly increase with depth, and the pH values slightly vary around 4.3. The sediments of the lowermost layers 4 to 1 (269–314 cm b.s.) show slightly increased TC concentrations compared to the layers above. This part of the profile shows markedly increasing EC values (54  $\mu\text{S cm}^{-1}$  at 271.5 cm depth), reaching the highest values (126  $\mu\text{S cm}^{-1}$  at 303.5 cm depth) in the lowermost layer 1 (297–314 cm b.s.) and showing a distinct decrease in the pH values to 3.0, which is comparably acidic to layer 25.

The concentrations of the elements Al, Si, and Fe generally show minor variation in the upper part of the profile (between layers 25 and 5) and major shifts in the lower part. The upper part of the profile is characterized by low Fe ( $\bar{x} = 0.5$  mass %;  $\sigma = 0.1$  mass %;  $n = 34$ ) and Al ( $\bar{x} = 1.7$  mass %;  $\sigma = 0.2$  mass %;  $n = 34$ ) contents, while the Si contents are high ( $\bar{x} = 43.8$  mass %;  $\sigma = 0.8$  mass %;  $n = 34$ ). The Si concentration starts to slightly decrease at the bottom of layer 5 and shows strongly decreased contents in layers 2 and 1 ( $\bar{x} = 29.7$  mass %;  $\sigma = 0.7$  mass %;  $n = 2$ ). Generally, the Al and Fe contents of the lower profile show the opposite course of the Si concentrations; the highest values are reached in layers 2 and 1 (Al:  $\bar{x} = 6.1$  mass %;  $\sigma =$

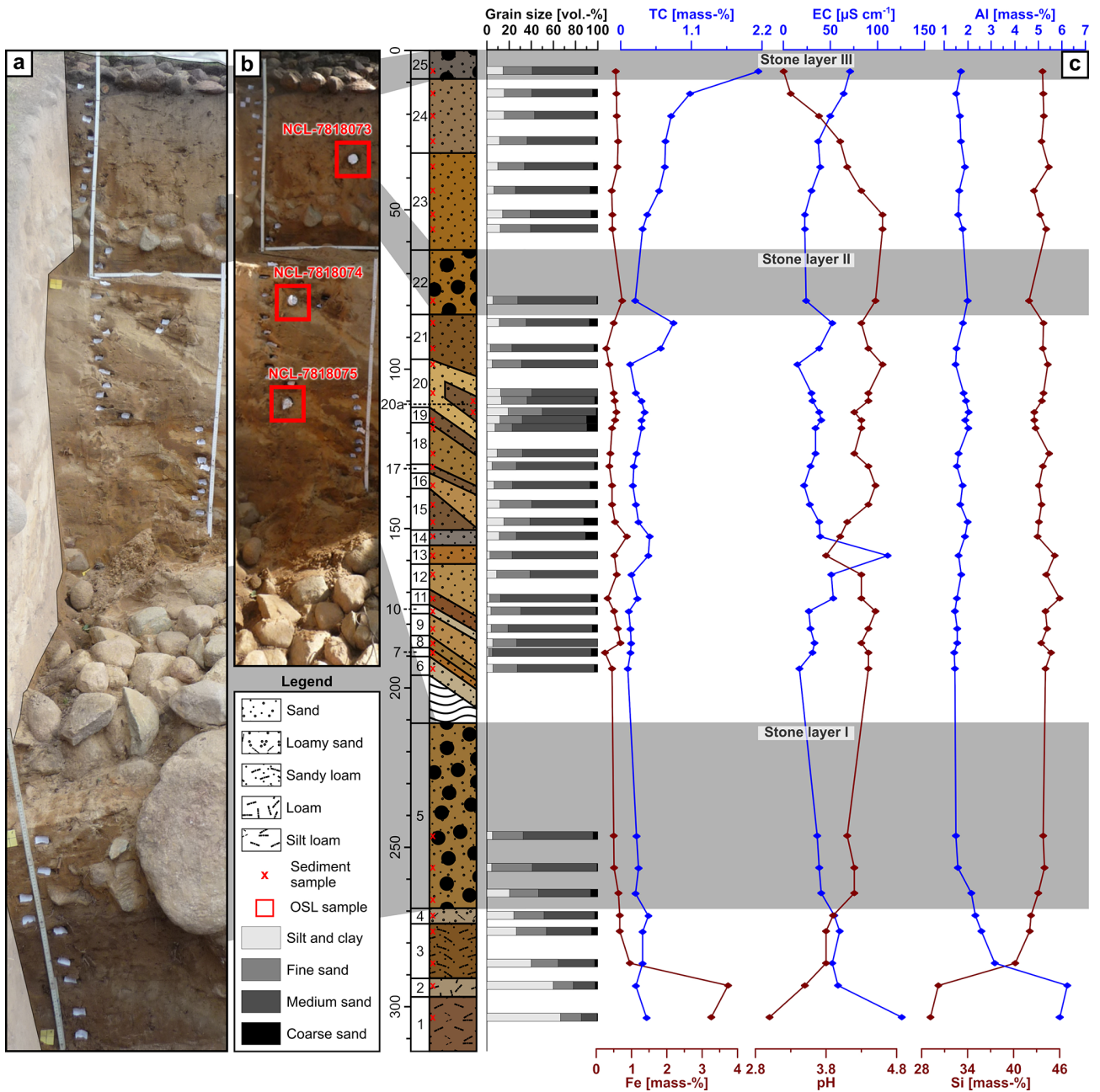


**Figure 5.** Composite illustration of (a) photograph of profile SD17P1 after description and sampling (the white labels in the photograph show the sampling spots); (b) profile photograph of the upper profile part highlighting the OSL sampling locations and sample IDs; and (c) schematic drawing with grain size composition and geochemical sediment parameters (TC is total carbon contents, EC is electrical conductivity, Al is aluminum, Fe is iron, Si is silicon).

0.2 mass %;  $n = 2$ ; Fe:  $\bar{x} = 3.5$  mass %;  $\sigma = 0.3$  mass %;  $n = 2$ ).

### 4.3 OSL ages

The results of paleodose and dose rate determination are listed in Table 1. The dose rates of the three samples vary between  $1.11 \pm 0.04$  Gy kyr<sup>-1</sup> to  $1.30 \pm 0.05$  Gy kyr<sup>-1</sup>, which is in the normal range for this kind of sediment. The paleodose of samples NCL-781873 and NCL-7818075 are significantly smaller than of NCL-781874. This suggests that the former two samples contain sand grains that can be associated with recent, thus most likely anthropogenic, reworking while sample NCL-7818074 shows a large paleodose (and thus age) that is most likely associated with the primary deposition of the sediments.

The corresponding ages indicate for the uppermost and the lowermost samples that the anthropogenic reworking occurred between  $4.5 \pm 1.0$  and  $3.1 \pm 0.7$  kyr ago. The errors associated with both samples are relatively large because the youngest dose population modeled by the bootMAM only represents a fraction of the total  $D_e$  distribution (see distributions in Fig. 6). It should be noted that OSL ages are reported with their  $1\sigma$  uncertainty and range between 3520 and 420 BCE. Based on the  $2\sigma$  confidence interval, the youngest age components of NCL-7818073 and NCL-7818075 that are again most likely associated with anthropogenic reworking range between 4520 BCE and 320 CE.

## 5 Discussion

### 5.1 Chronological framework

The sediment layers bracketed by the stone pavements contain sand-sized quartz well suited for OSL dating. With OSL dating, we ideally determine the time when these sediments were last reworked (presumably by humans). The idea is that during this anthropogenic reworking some grains were exposed to light. Using OSL dating we are able to determine the burial age associated with this last reworking event (e.g., van der Meij et al., 2019). OSL samples NCL-7818073 and NCL-7818075 (layer 23 and layer 12, respectively) show large variations in their corresponding small aliquot  $D_e$  distributions (Fig. 6) with (i) large  $D_e$  values likely representing the original deposition of glaciofluvial or coversand deposits and (ii) very small  $D_e$  values (of <10 Gy) most likely being associated with anthropogenic reworking. It should be noted at this point that our 1 mm aliquots are regarded, at least in this sedimentary setting, as reliable proxies for genuine single-grain OSL analyses (e.g., Lüthgens et al., 2011; Reimann et al., 2012). Therefore, the calculated bootMAM ages derived from the youngest  $D_e$  population of samples NCL-7818073 and NCL-7818075 point at an anthropogenic reworking age of 2.4–5.5 ka ( $1\sigma$  confidence interval). This age range is in good agreement with the radiocarbon ages

and the archeological evidence, i.e., the suggested time span for period V (Hornstrup et al., 2012). Additionally, the three radiocarbon ages from the fossil soil layer below the basal stone layer I yield a similar age range and a terminus post quem time frame for the construction of the burial mound of 910–800 BCE (Table 2).

The age error that we had to assign to both ages is relatively large ( $\sim 22\%$ ) compared to OSL ages from well-bleached and unmixed samples that typically show smaller age errors between 5 to 10%. These large errors reflect the complexity of the corresponding  $D_e$  distributions of samples NCL-7818073 and NCL-7818075, more precisely the small fraction of  $D_e$  values that were used to calculate the paleodose associated with the anthropogenic reworking. However, it should be noted that the youngest age components in the uppermost and lowest samples both fall into the radiometric age of the construction site even though the OSL ages reflect rather large error bars. We assume that the construction of the sediment packages between the stone pavements was done within a rather short time frame and material was taken from continuously used pits. However, based on the OSL ages and due to non-calculable factors such as the number of individuals involved in the construction or the equipment they used, it is not possible to provide a time estimate for the duration of the construction process.

Sample NCL-7818074 (layer 20) contains no young grains in its  $D_e$  distribution, suggesting that during anthropogenic reworking no or too few sand grains were surfaced, and thus this reworking event was not able to leave an imprint on the corresponding  $D_e$  distribution.

Interestingly, anthropogenic reworking of the sediment packages only produced incompletely mixed samples presumably linked to the corresponding construction technique. While we can use the paleodose of the youngest dose population to estimate the timing of the anthropogenic disturbance (outlined above), we can use the number of aliquots in this population, which is assumed to be proportional to mixing intensity (Reimann et al., 2017), as a fingerprint of the construction technique that produced the disturbance. From the  $D_e$  distribution shown in Fig. 6, it appears that the uppermost sample NCL-7818073 (at  $\sim 0.52$  m depth) contains more grains in the younger population than that of the lowest sample NCL-7818075 (at  $\sim 1.68$  m depth). This may point to a different way of constructing the upper part of the section presumably characterized by more intensive grain surfacing. Alternatively, this observation might be linked to subsequent soil formation and thus grain surfacing through bioturbation.

Looking at the older population of the complex  $D_e$  distributions (Fig. 6), we can also learn something about the primary deposition(s) of the sandy material (e.g., Huisman et al., 2019). The middle sample NCL-7818074 ( $\sim 1.22$  m depth) is dominated by aliquots with  $D_e$  values well above 100 Gy which can be associated with the deposition of glaciofluvial sand during the late Saalian. Furthermore, we can observe younger aliquots below 100 Gy, pos-

**Table 1.** OSL dating results (n/a is no answer). See Sects. 3.3 and 4.3 for details.

NCL Code	Sample ID	Depth (m)	Paleodose (Gy)	Dose rate (Gy kyr <sup>-1</sup> )	Age (ka)	Date (BCE)	Systematic	Random	Reliability	Comments
NCL-7818073	SD17P1 53	0.52	4.1 ± 0.9	1.29 ± 0.05	3.1 ± 0.7	1120 ± 700	0.12	0.67	Likely OK	
NCL-7818074	SD17P1 125	1.22	153 ± 11	1.11 ± 0.04	138 ± 11	n/a	5.29	10.09	Inaccurate	Not bleached
NCL-7818075	SD17P1 170	1.68	5.9 ± 1.3	1.30 ± 0.05	4.5 ± 1.0	2520 ± 1000	0.17	1.04	Questionable	Too few young aliquots

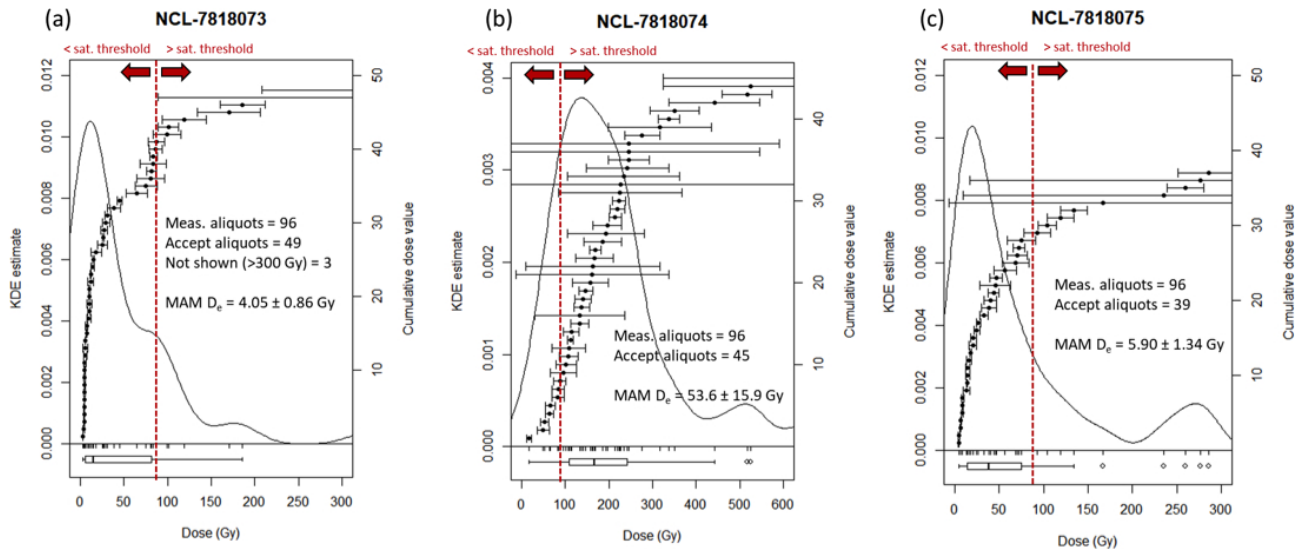


**Figure 6.** (a) to (c)  $D_e$  distribution of the three OSL samples shown as kernel density plots (KDEs). Dashed red line represents the average lower threshold of OSL signal saturation (2D0 value is sat. threshold) which was estimated based on the dose response curves to ~90 Gy. For  $D_e$  values to the right of this dashed line, it is not possible to calculate an accurate age. Although the face value of these large  $D_e$  values needs to be taken with caution, they provide insights into (i) the approximate age and (ii) the fraction of grains that have not been surfaced since approximately the early Weichselian. Note that the  $x$  axis for (b) is different from (a) and (c).

sibly associated with the reworking of the sediment package during the early to middle Weichselian related to either periglacial processes (cryoturbation) or soil mixing (bioturbation) during interstadials. The uppermost and the lowermost samples (NCL-7818073, NCL-7818075) also seem to recover the late Saalian and Weichselian aliquot populations.

## 5.2 Interpretation of the site and landscape context

Our results are in good agreement with previous studies regarding the prevailing substrates and their middle to late Quaternary history of deposition and reworking. The silty loam and loam deposits of layers 2 and 1 have substantially reduced sand contents in favor of increased silt and clay contents. This is also supported by the substantially increased Fe and Al contents, together with the considerably decreased Si values within these layers compared to the top layers that generally show minor variations for these elements (Fig. 5c). These layers are regarded as presenting late Saalian till de-

posits (Fig. 7a) that form part of the slightly undulating till plains in the old morainic area of the Prignitz region (Lippstreu et al., 1997; Nagel et al., 2003; Lippstreu et al., 2015; Fig. 2a). Next to the till plains, late Saalian glaciofluvial sand plains (Fig. 7a) form a major landscape component in the surroundings of the royal tomb (Königsgrab) of Seddin, and the overlying layers 3 and 4 correspond to the sandy to loamy-sandy deposits that commonly cover the till deposits (GeoBasis-DE/LGB, 2012; Fig. 2a). Periglacial reworking of these deposits and coversand formation occurred during the Weichselian (Kasse, 2002; Nagel et al., 2003; Koster, 2005; Kaiser et al., 2009; Lüthgens et al., 2010; Fig. 7b) and soil formation, in conjunction with the development of the vegetation cover, during the late glacial and Holocene (Kühn, 2003; Kappler et al., 2019; Fig. 7c).

During the Bronze Age, the landscape in Brandenburg opened substantially due to large-scale woodland clearings especially during the Late Bronze Age (Jahns, 2015, 2018).

**Table 2.** Comparison of  $^{14}\text{C}$  and OSL ages.

Laboratory ID	Material	$^{14}\text{C}$ age (years BP)	Uncertainty (years)	Age	Age	Reference
				( $2\sigma$ ; from–to cal. a BP)	( $2\sigma$ ; from–to BCE)	
KIA 21317 <sup>a</sup>	<i>Salix/Populus/Quercus</i>	2694	31	2851–2754	902–805	May (2018)
MAMS 35030 <sup>a</sup>	<i>Fagus</i>	3375	22	3688–3570	1739–1621	This study
MAMS 21017 <sup>a</sup>	<i>Pinus</i>	2719	19	2855–2769	906–820	May (2018)
MAMS 21018 <sup>a</sup>	<i>Corylus</i>	2725	19	2859–2773	910–824	May (2018)
		Paleodose (Gy)	Dose rate (Gy kyr <sup>-1</sup> )	Age (1 $\sigma$ ; ka)	Age (1 $\sigma$ ; BCE)	
NCL-7818073 <sup>b</sup>	Purified quartz-rich extracts (212–250 $\mu\text{m}$ )	4.1 $\pm$ 0.9	1.29 $\pm$ 0.05	2400–3800	420–1820	This study
NCL-7818075 <sup>b</sup>	Purified quartz-rich extracts (212–250 $\mu\text{m}$ )	5.9 $\pm$ 1.3	1.30 $\pm$ 0.05	3500–5500	1520–3520	This study

<sup>a</sup> Radiocarbon ages were obtained from charcoal pieces recovered from layers that stratigraphically correspond to layer 23 of profile SD17P1 yielding the terminus post quem time frame for the construction of the burial mound; <sup>b</sup> OSL ages from the deposits of the burial mound providing direct age estimates for the construction phases.

The charcoals obtained from the substrate below the burial mound (Table 2) suggest that the local forest composition at the construction site prior to the initial construction phase in the Late Bronze Age included pine (*Pinus*), hazel (*Corylus*), and either willow (*Salix*), poplar (*Populus*), or oak (*Quercus*).

A comparison of the grain size distributions of the layers that form the burial mound (layers 5–25) and the geological, soil type, and texture maps (Fig. 2) indicate that the mound most likely was exclusively constructed from glaciofluvial sand – except for the erratic boulders forming the three stone layers. The first stone pavement is regarded as representing the first material that was deposited during the initial construction phase of the alternating stone and sand strata, and May (2018) suggests that the substrate below stone layer I represents a fossil soil that was buried during this initial construction phase (Fig. 7d). The dark material that was recorded during several archeological excavations underneath stone layer I (May, 2018) stratigraphically corresponds to layer 3 in profile SD17P1. Our geochemical sediment analyses support the assumption of May (2018) as the TC values very slightly increase below layer 5, the pH values are reduced in layers 4 and 3 compared to layer 5, and the electric conductivity is concurrently increased (Fig. 5c). However, the increased EC values might result from a grain-size effect as the texture becomes finer towards the base of the profile. As these characteristics roughly resemble the horizon characteristics of a typical Fahlerde or Braunerde-Fahlerde in this part of the Prignitz–Brandenburg region (MLUV, 2005), we interpret layer 4 as the fAel horizon and layer 3 as the fBt horizon (according to Ad-Hoc-AG Boden, 2005). According to the soil classification system of the IUSS Working Group WRB (2006), this corresponds to a Luvisol with layer 4 being the fossil albic horizon and layer 3 being the underlying fossil argic horizon. This soil horizon designation also sug-

gests that the soil profile is truncated and that a fAh horizon is missing below stone layer I. The missing fossil, organic-rich topsoil horizon (fAh horizon) was already recorded at several locations below the mound; it was pointed out that either a “dark substrate” or a “pale solidified sand” occurs directly underneath the lowermost stone pavement, i.e., in stratigraphically identical positions (May, 2018). Based on the present results, we assume that the “dark substrate” from the archeological descriptions represents the fBt horizon and the “pale solidified sand” the fAel horizon showing an irregular occurrence below stone layer I. On the one hand, the absence of the fAh horizon and partially also of the fAel horizon may be the result of soil erosion by water or wind after the surface of the construction site was cleared of vegetation; the sandy material of the fAh and fAel horizons is more susceptible to erosion compared to the loamy material of the fBt horizon below. On the other hand, intentional leveling of the construction ground after vegetation clearance but before the deposition of stone layer I might have caused the removal of the topsoil horizon(s). Both scenarios are supported by the archeological observation that pieces of charcoal and ceramic are incorporated into the fAel and the fBt horizons below the mound, indicating that the soil surface was disturbed during the Late Bronze Age construction of the burial mound. It seems very likely that the erosion or removal of the topsoil horizon(s) occurred closely before the initial construction phase of the royal tomb, but at present, we have no evidence to favor either of these scenarios.

At a Bronze Age burial mound site in Denmark (Lejrskov), Holst et al. (1998) also describe a buried soil beneath the mound structure. The fossil A horizon at their site has a little more than 0.5 % of organic matter. They argue that the organic matter content could have been higher but might be subjected to decomposition since burial.

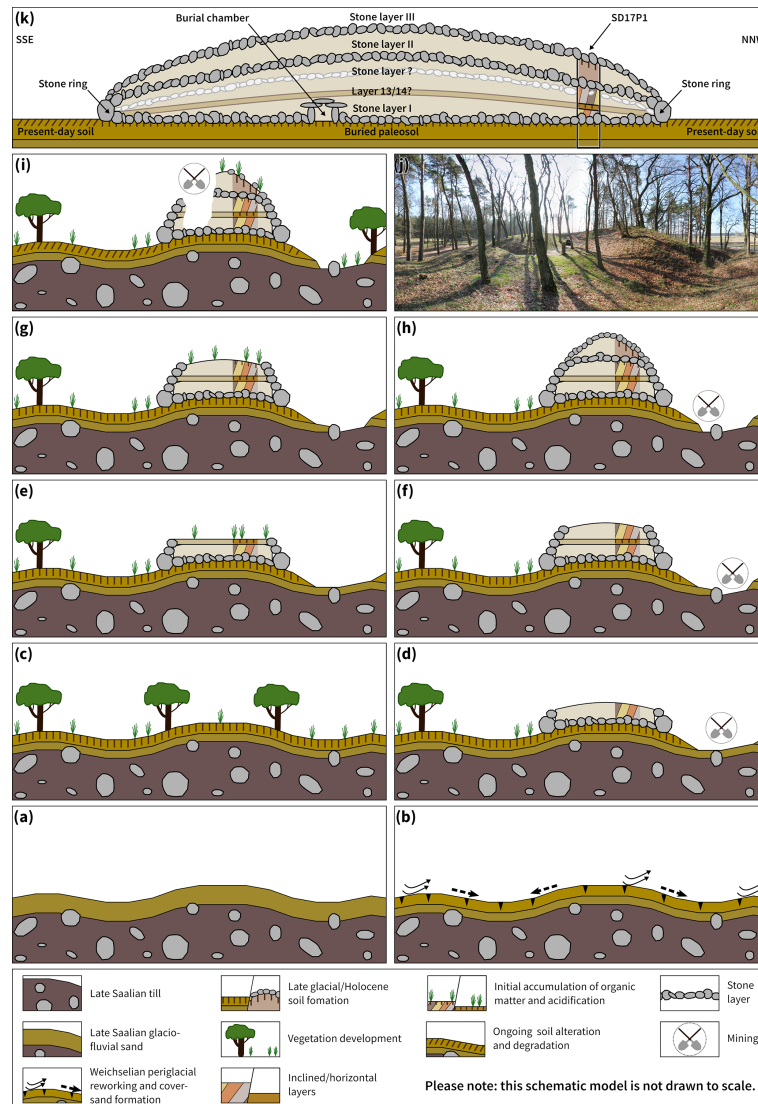


**Figure 7.** Schematic genetic model of the late Saalian to Holocene landscape development, possible construction phases of the burial mound, and its present-day schematic concept according to the state of the art (cf. locations of the excavation trenches in Fig. 3). During the late Saalian, till was deposited and partly covered by glaciofluvial deposits (a). Periglacial reworking and cover sand formation occurred during the Weichselian (b). During the late glacial and Early Holocene, a denser vegetation cover developed, and soil formation occurred (c). With the start of the construction of the burial mound, the soil was truncated, and its remaining fAel and fBt horizons were buried underneath the first stone pavement; the overlying sand packages show late Saalian and Weichselian, as well as Holocene, OSL ages, the latter being linked to anthropogenic reworking (d). After the first construction phase, weedage may have occurred that would allow for the initial accumulation of organic matter (e). The sand package of the second construction phase solely shows a late Saalian OSL age (f). Weedage and initial accumulation of organic matter may also have occurred after the second construction phase (g). The second stone pavement, the uppermost sand package, and the surface-covering stone pavement were presumably deposited during a third construction phase; the sand packages show late Saalian and Holocene OSL ages (h). The paleosol recorded underneath the burial mound is not preserved in the area around, but soil development continued, and the soil was modified and degraded by land use such as plowing and sediment extraction. Gravel mining in the late 19th century partially destroyed the burial mound (i), but heritage protection measures preserved the archeological remains until the present day (j). The presented schematic genetic model (d–i) is based on the results of profile SD17P1 and is simplified compared to the schematic concept according to the state of the art (k). The manifestation of particular characteristics such as the two packages of inclined layers or the two horizontal layers in between vary locally. Also, some of the excavation trenches yielded indications for an additional stone layer between stone layers I and II (k). Please note that the location(s) of the sand pit(s) that were exploited to construct the burial mound have not been identified and are presented idealized here.

Other studies carried out in the context of Bronze Age burial mounds focused on paleosols as a proxy for paleoenvironmental conditions during the times of usage of the mounds. At a site in northern Germany (Bornhöved), Dreibrodt et al. (2009) suggest that the surrounding area was probably forested during the time. In contrast, at a burial mound site in southern Sweden (Bjäre peninsula), a significant decrease in forest coverage was reconstructed for the respective time of usage (Hannon et al., 2008).

The particular geochemical properties as described above (i.e., layers with increased TC contents, high electric conductivity values, and decreased pH values) also occur in layers 14–13, 21, and 25–24. These characteristics may point to phases when humic acids, together with a higher availability of soluble salts, may have occurred in conjunction with humus accumulation. This interpretation is supported by the particular signature of the values, i.e., the TC values decrease with increasing depth, which is a typical feature of soil development. The results of Haburaj et al. (2020) support this interpretation, too. They study the upper part of the same excavation trench and combine data from RGB and multispectral cameras, visible and near-infrared hyperspectral data, and geochemical data. Their image classifications show that soil organic carbon is mainly increased in layers 24, 21, and 14 (according to the layer counting presented here) and that these layers run more or less horizontally along the entire width of the excavation trench (Haburaj et al., 2020). Even though these arguments support the interpretation of initial in situ accumulation of organic matter, inherited sediment properties from reworked material cannot be excluded.

These characteristics occur three times in our profile (Fig. 5). First, it (Fig. 7e) occurs in the horizontally bedded layers 14 and 13 that overly the lowermost package of inclined layers (12–6). The upper package of inclined layers (15–21) bury the two horizontal layers (Fig. 7f). Within the sediments of layer 21, which represents the final stage of sand accumulation below stone layer II (Fig. 7g), the initial accumulation of organic matter, increasing acidity, and higher availability of soluble salts occur again. We interpret this as an indication for phases when the construction works possibly were interrupted for a short, yet not further definable, period of time. Such an interruption of the construction process likely would have allowed the development of an initial vegetation cover due to weedage and as a consequence the accumulation of organic matter. The inclined structure of layers 12–6 and 21–15 are clearly visible in section SD17P1. This is not necessarily the case throughout the entire burial mound as other sections that were opened did not display this structure so distinctly. Such locally varying characteristics are also documented for other burial mounds (e.g., Holst and Rasmussen, 2015). These sediments are buried by the second stone pavement, the uppermost sand package (layers 23–24), and stone layer III (Fig. 7h). The properties of layers 25–23 presumably represent the result of ongoing soil formation processes that started from the completion of the

Late Bronze Age burial mound, also as a consequence of post-Bronze-Age vegetation development on top of the burial mound. Intensive exploitation of rock and sand in the course of the late 19th century led to the partial destruction of the burial mound (Fig. 7i) and ultimately to its discovery in the year 1899 (May, 2018). Restoration and the planting of trees started at the beginning of the 20th century (May, 2018), preserving the remains of the monumental burial mound royal tomb (Königsgrab) of Seddin (Fig. 7j).

### 5.3 Opportunities and challenges of a minimal invasive approach for OSL dating of burial mounds

As shown by Kristiansen et al. (2003), augering through burial mounds can yield material from buried organic-rich topsoil horizons suitable for the  $^{14}\text{C}$  analysis of soil organic matter fractions. An absent or fragmentarily preserved organic-rich topsoil horizon below the mound – as is the case for the profile presented here – would cause problems. Sand-sized quartz grains, in contrast, are ubiquitous in the European sand belt, and probably most, if not all, burial mounds contain it as a fraction of their construction material. Therefore, we propose to modify the approach of Kristiansen et al. (2003) and suggest to rather use engine-driven vibracoring techniques instead of augering to obtain undisturbed sediment cores from the body of the burial mound and the (possibly) underlying buried soil in plastic tubes. In doing so, datable material for  $^{14}\text{C}$  analysis from a possibly present buried organic-rich topsoil horizon and sand-sized quartz grains from the burial mound itself suitable for OSL dating can be obtained. It has been shown that samples for OSL dating can be obtained from plastic liners that were driven into the subsurface by means of steel probes (e.g., Reimann et al., 2010, 2012).

Our first attempt to use OSL dating of sand-sized quartz grains to determine the construction period of a burial mound generally shows good applicability of this approach but also reveals challenges (cf. also Porat et al., 2012; Pluckhahn et al., 2015; al Khasawneh et al., 2020). One of the main challenges is the relatively large error of ca. 22 % compared to errors of 5 %–10 % that are typical for well-bleached and un-mixed samples. Therefore, the clear temporal association of a burial mound to a specific cultural epoch can be problematic. One solution to reduce this error and thus possibly date newly discovered burial mounds more accurately would be the use of single-grain feldspar luminescence instead. Sand-sized feldspar grains typically occur in various Quaternary deposits along the European sand belt (e.g., Füchtbauer and Elrod, 1971; Saye and Pye, 2006; Kalińska-Nartiša et al., 2015; Kaliniska et al., 2019), and Reimann et al. (2017) have shown that this novel method holds important advantages over quartz single-grain OSL in settings with a complex history of reworking. In a burial mound setting as presented in this study, it might be possible to reduce the age error to 6 %–7 % using single-grain feldspar luminescence.

## 6 Conclusions

Our OSL chronology – on account of its much larger age range – matches the radiocarbon-based terminus post quem time frame of 910–800 BCE for the construction period of the monumental burial mound royal tomb (Königsgrab) of Seddin and therewith supports its chronological affiliation to the transition from the Late Bronze Age to the Iron Age now with process-based datings. Beyond this temporal correspondence with the construction period, our OSL ages also provide new temporal insights into the initial deposition of late Saalian glaciofluvial sand and its Weichselian periglacial reworking. Our initial experiences with the OSL dating of sediments from a burial mound have revealed its generally good applicability but also related challenges. Based on our experiences, we have proposed a minimal invasive approach to obtain samples for  $^{14}\text{C}$  and OSL dating that can be tested on well-studied burial mounds and may help to provide initial numerical age control for newly discovered ones.

The presented results of the sedimentological and geochemical analyses prove the existence of a truncated paleosol underneath the lowermost stone pavement of the tomb. The two identified fossil horizons are interpreted as fAel and fBt horizons of a Fahlerde or Braunerde-Fahlerde, i.e., fossil albic and fossil argic horizons of a Luvisol, which is a typical soil in this part of the Prignitz region. At three locations of the upper part of the profile (layers 14–13, 21, and 25–24), increased TC and electric conductivity values and decreased pH values occur. This may point to the in situ enrichment of humus, soluble salts, and humic acids as a consequence of possible phases when the construction works were likely interrupted and weedage occurred.

**Data availability.** Additional information on the applied methods, quality control measures, and the sedimentological and geochemical data are provided in the Supplement.

**Supplement.** The supplement related to this article is available online at: <https://doi.org/10.5194/egqsj-70-1-2021-supplement>.

**Author contributions.** This study was designed by MN, PH, and JM who also carried out field work. Luminescence dating was done by TR. MN wrote the paper; JH, PH, JM, and TR provided contributions. All authors read, commented on, and approved the paper and the revised version.

**Competing interests.** The authors declare that they have no conflict of interest.

**Acknowledgements.** This study is funded by the Excellence Cluster (EXC 264) Topoi – The Formation and Transformation of

Space and Knowledge in Ancient Civilizations. We acknowledge support from the open-access publication fund of Freie Universität Berlin. The authors very much appreciate the technical support from Erna Voskuilen during the OSL analyses and Lena Schimmel and Vincent Haburaj during field work. We express our sincere thanks to Knut Kaiser and an anonymous reviewer for thoroughly evaluating our paper. Their constructive comments and criticisms helped to critically reflect and clarify some aspects of this study; detailed suggestions enhanced its value. Markus Fuchs is acknowledged for handling our paper as associate editor.

**Financial support.** This research has been supported by the Deutsche Forschungsgemeinschaft (DFG) (grant no. 39235742).

We acknowledge support from the open-access publication initiative of Freie Universität Berlin.

**Review statement.** This paper was edited by Markus Fuchs and reviewed by Dr. Knut Kaiser and one anonymous referee.

## References

- Ad-Hoc-AG Boden: *Bodenkundliche Kartieranleitung*, Schweizerbart, Stuttgart, 2005 (in German).
- Aitken, M. J.: *Thermoluminescence Dating*, Academic Press Inc. Ltd, London, 1985.
- al Khasawneh, S., Murray, A., Kafafi, Z., and Petit, L.: Luminescence Dating of the Iron Age Deposits from Tell Damiyah in the Jordan Valley, *Radiocarbon*, 62, 1–12, 2020.
- Beck, H. E., Zimmermann, N. E., McVicar, T. R., Vergopolan, N., Berg, A., and Wood, E. F.: Present and future Köppen-Geiger climate classification maps at 1-km resolution, *Scientific Data*, 5, 180214, <https://doi.org/10.1038/sdata.2018.214>, 2018.
- Böse, M., Lüthgens, C., Lee, J. R., and Rose, J.: Quaternary glaciations of northern Europe, *Quatern. Sci. Rev.*, 44, 1–25, 2012.
- Cunningham, A. C. and Wallinga, J.: Selection of integration time intervals for quartz OSL decay curves, *Quat. Geochronol.*, 5, 657–666, 2010.
- Cunningham, A. C., DeVries, D. J., and Schaart, D. R.: Experimental and computational simulation of beta-dose heterogeneity in sediment, *Radiat. Meas.*, 47, 1060–1067, 2012.
- Doorenbosch, M.: *Ancestral heaths: reconstructing the barrow landscape in the Central and Southern Netherlands*, Sidestone Press, Leiden, the Netherlands, 2013.
- Dreibrodt, S., Nelle, O., Lütjens, I., Mitusov, A., Clausen, I., and Bork, H.-R.: Investigations on buried soils and colluvial layers around Bronze Age burial mounds at Bornhöved (northern Germany): an approach to test the hypothesis of “landscape openness” by the incidence of colluviation, *Holocene*, 19, 487–497, 2009.
- DWD Climate Data Center: Annual mean of Station observations of air temperature at 2 m above ground in °C for Germany, version v19.3., available at: <https://cdc.dwd.de/portal/> (last access: 15 July 2020), 2020a.

- DWD Climate Data Center: Annual station observations of precipitation in mm for Germany, version v19.3., available at: <https://cdc.dwd.de/portal/> (last access: 15 July 2020), 2020b.
- Ehlers, J., Grube, A., Stephan, H.-J., and Wansa, S.: Pleistocene Glaciations of North Germany–New Results, in: Quaternary Glaciations – Extent and Chronology. A Closer Look, Developments in Quaternary Science, 15, edited by: Ehlers, J., Gibbard, P. L., and Hughes, P. D., Elsevier, Amsterdam, the Netherlands, 149–162, 2011.
- European Environment Agency: Corine Land Cover (CLC) 2018, Version 2020\_20u1, available at: <https://land.copernicus.eu/pan-european/corine-land-cover/clc2018>, last access: 15 July 2020.
- Feathers, J. K.: Luminescence dating of early mounds in Northeast Louisiana, *Quaternary Sci. Rev.*, 16, 333–340, 1997.
- Füchtbauer, H. and Elrod, J. M.: Different sources contributing to a beach sand, southeastern Bornholm (Denmark), *Sedimentology*, 17, 69–79, 1971.
- Galbraith, R. F., Roberts, R. G., Laslett, G. M., Yoshida, H., and Oley, J. M.: Optical dating of single and multiple grains of quartz from Jinnium rock shelter, Northern Australia: part 1, experimental details and statistical models, *Archaeometry*, 41, 339–364, 1999.
- GeoBasis-DE/LGB: Bodenübersichtskarte des Landes Brandenburg 1:300 000, available at: <http://www.geo.brandenburg.de/boden/> (last access: 21 April 2020), 2012 (in German).
- GeoBasis-DE/LGB: Digitales Geländemodell, available at: <https://data.geobasis-bb.de/geobasis/daten/dgm/xyz/>, last access: 21 April 2020 (in German).
- Geofabrik: Brandenburg (mit Berlin), available at: <http://download.geofabrik.de/europe/germany.html>, last access: 21 April 2020.
- Guérin, G., Mercier, N., and Adamiec, G.: Dose rate conversion factors: update, *Ancient TL*, 29, 5–8, 2011.
- Haburaj, V., Nykamp, M., May, J., Hoelzmann, P., and Schütt, B.: On-Site VIS-NIR Spectral Reflectance and Colour Measurements—A Fast and Inexpensive Alternative for Delineating Sediment Layers Quantitatively? A Case Study from a Monumental Bronze Age Burial Mound (Seddin, Germany), *Heritage*, 3, 528–548, 2020.
- Hannon, G. E., Bradshaw, R. H. W., Nord, J., and Gustafsson, M.: The Bronze Age landscape of the Bjäre peninsula, southern Sweden, and its relationship to burial mounds, *J. Archaeol. Sci.*, 35, 623–632, 2008.
- Harding, A.: The Tumulus in European Prehistory: Covering the Body, Housing the Soul, in: Ancestral Landscape. Burial mounds in the Copper and Bronze Ages, Proceedings of the International Conference, Udine, Italy, 15–18 May 2008, 21–30, 2012.
- Holst, M. K. and Rasmussen, M.: Skelhøj and the Bronze Age barrows of southern Scandinavia, *Jut. Arch. Soc. Pub.*, 78, Aarhus University Press, Aarhus, Denmark, 2015.
- Holst, M. K., Breuning-Madsen, H., and Olsson, M.: Soil Forming Processes in and below a Bronze Age Burial Mound at Lejrskov, Southern Jutland, *Geogr. Tidsskr.*, 98, 46–55, 1998.
- Hornstrup, K. M., Olsen, J., Heinemeier, J., Thrane, H., and Bennike, P.: A new absolute Danish Bronze Age chronology as based on radiocarbon dating of cremated bone samples from burials, *Acta Archaeol.*, 83, 5–53, 2012.
- Huisman, H., de Kort, J.-W., Ketterer, M. E., Reimann, T., Schoorl, J. M., van der Heiden, M., van Soest, M., and van Egmond, F.: Erosion of archaeological sites: Quantifying the threat using optically stimulated luminescence and fallout isotopes, *Geoarchaeology*, 34, 478–494, 2019.
- IUSS Working Group WRB: World Reference Base for Soil Resources 2006, World Soil Resources Reports No. 103, FAO, Rome, Italy, 2006.
- Jahns, S.: Bronze Age settlements reflected in pollen diagrams from Brandenburg, Eastern Germany, in: The third food revolution? Setting the Bronze Age table: common trends in economic and subsistence strategies in Bronze Age Europe, edited by: Kneisel, J., Dal Corso, M., Kirleis, W., Scholz, H., Taylor, N., and Tiedtke, V., Habelt, Bonn, Germany, 237–248, 2015.
- Jahns, S.: Pollenanalytische Untersuchungen zur Bronzezeit am Bergsoll bei Helle, Lkr. Prignitz, in: Der Grabhügel von Seddin im norddeutschen und südkandinavischen Kontext, Arbeitsberichte zur Bodendenkmalpflege in Brandenburg, 33, edited by: Hansen, S. and Schopper, F., Brandenburgisches Landesamt für Denkmalpflege und Archäologisches Landesmuseum, Wünsdorf, Germany, 85–90, 2018 (in German).
- Kaiser, K., Hilgers, A., Schlaak, N., Jankowski, M., Kühn, P., Bussemer, S., and Przegiętka, K.: Palaeopedological marker horizons in northern central Europe: characteristics of Lateglacial Usselo and Finow soils, *Boreas*, 38, 591–609, 2009.
- Kaiser, K., Schneider, T., Küster, M., Dietze, E., Fülling, A., Heinrich, S., Kappler, C., Nelle, O., Schult, M., Theuerkauf, M., Vogel, S., de Boer, A. M., Börner, A., Preusser, F., Schwabe, M., Ulrich, J., Wirner, M., and Bens, O.: Palaeosols and their cover sediments of a glacial landscape in northern central Europe: Spatial distribution, pedostratigraphy and evidence on landscape evolution, *Catena*, 193, 104647, <https://doi.org/10.1016/j.catena.2020.104647>, 2020.
- Kaliniska, E., Hang, T., JoBeleht, A., Olo, S., Nartišs, M., and Adamiec, G.: Macro- and micro-scale study and chronology of Late Weichselian aeolian sediments in Estonia, north-eastern European Sand Belt, *Int. J. Earth Sci.*, 108, 2021–2035, 2019.
- Kaliniska-Nartiša, E., Thiel, C., Nartišs, M., Buylaert, J.-P., and Murray, A. S.: Age and sedimentary record of inland eolian sediments in Lithuania, NE European Sand Belt, *Quaternary Res.*, 84, 82–95, 2015.
- Kappler, C., Kaiser, K., Küster, M., Nicolay, A., Fülling, A., Bens, O., and Raab, T.: Late Pleistocene and Holocene terrestrial geomorphodynamics and soil formation in northeastern Germany: a review of geochronological data, *Phys. Geogr.*, 40, 405–423, 2019.
- Kasse, C.: Sandy aeolian deposits and environments and their relation to climate during the Last Glacial Maximum and Lateglacial in northwest and central Europe, *Prog. Phys. Geogr.*, 26, 507–532, 2002.
- Kiekebusch, A.: Das Königsgrab von Seddin, Führer zur Urgeschichte, Benno Filser, Augsburg, Germany, 1928 (in German).
- Kossinna, G.: Ansprache über die "Kulturgeschichtliche Stellung der Prignitz in der Vorzeit", *Mannus Zeitschrift für Vorgeschichte*, 2, 234–240, 1910 (in German).
- Koster, E. A.: Recent Advances in Luminescence Dating of Late Pleistocene (Cold-Climatic) Aeolian and Loess Deposits in Western Europe, *Permafrost Periglac.*, 16, 131–143, 2005.
- Kristiansen, S. M., Dalsgaard, K., Holst, M. K., Aaby, B., and Heinemeier, J.: Dating of prehistoric burial mounds by  $^{14}\text{C}$  anal-

- ysis of soil organic matter fractions, *Radiocarbon*, 45, 101–112, 2003.
- Kühn, P.: Micromorphology and Late Glacial/Holocene genesis of Luvisols in Mecklenburg-Vorpommern (NE-Germany), *Catena*, 54, 537–555, 2003.
- LBGR Brandenburg: Geologische Karte 1:25.000, available at: <http://www.geo.brandenburg.de/gk25>, last access: 16 July 2020 (in German).
- Lippstreu, L., Hermsdorf, N., and Sonntag, A.: Geologische Übersichtskarte des Landes Brandenburg 1:300 000, Landesamt für Geowissenschaften und Rohstoffe Brandenburg, Potsdam, Germany, 1997 (in German).
- Lippstreu, L., Hermsdorf, N., Sonntag, A., and Strahl, J.: Pleistozän, in: *Geologie von Brandenburg*, edited by: Stackebrandt, W. and Franke, D., Schweizerbart'sche Verlagsbuchhandlung, Stuttgart, Germany, 333–419, 2015 (in German).
- Litt, T., Behre, K.-E., Meyer, K.-D., Stephan, H.-J., and Wansa, S.: Stratigraphical Terms for the Quaternary of the North German Glaciation Area, *E G Quaternary Sci. J.*, 56, 7–65, 2007.
- Lüthgens, C., Böse, M., and Krbetschek, M.: On the age of the young morainic morphology in the area ascribed to the maximum extent of the Weichselian glaciation in north-eastern Germany, *Quatern. Int.*, 222, 72–79, 2010.
- Lüthgens, C., Böse, M., and Preusser, F.: Age of the Pomeranian ice marginal position in north-eastern Germany determined by Optically Stimulated Luminescence (OSL) dating of glaciofluvial (sandur) sediments, *Boreas*, 40, 598–615, 2011.
- May, J.: Neue Forschungen am “Königsgrab” von Seddin, in: *Der Grabhügel von Seddin im norddeutschen und südsandinavischen Kontext*, Arbeitsberichte zur Bodendenkmalpflege in Brandenburg, 33, edited by: Hansen, S. and Schopper, F., Brandenburgisches Landesamt für Denkmalpflege und Archäologisches Landesmuseum, Wünsdorf, Germany, 9–35, 2018 (in German).
- May, J. and Hauptmann, T.: Seddin, in: *Reallexikon der Germanischen Altertumskunde*, 28, edited by: Beck, H., Steuer, H., and Timpe, D., De Gruyter, Berlin, Germany, 1–6, 2005 (in German).
- May, J. and Hauptmann, T.: Warum befindet sich das “Königsgrab” von Seddin am Mittellauf der Stepenitz?, *Wasserwege und archäologische Sachkultur der jüngeren Bronzezeit in der Prignitz, Siedlungs- und Küstenforschung im südlichen Nordseegebiet*, Verlag Marie Leidorf GmbH, Rahden/Westfalen, Germany, 34, 129–150, 2011 (in German).
- May, J. and Hauptmann, T.: Das “Königsgrab” von Seddin und sein engeres Umfeld im Spiegel neuer Feldforschungen, in: *Gräberlandschaften der Bronzezeit, Bodenaltertümer Westfalens*, 51, edited by: Bérenger, D., Philipp von Zabern, Darmstadt, Germany 77–104, 2012 (in German).
- Mejdahl, V.: Thermoluminescence dating: beta-dose attenuation in quartz grains, *Archaeometry*, 21, 61–72, 1979.
- MLUV (Ministerium für Ländliche Entwicklung, Umwelt und Verbraucherschutz): Braunerde-Fahlerde. Steckbriefe Brandenburger Böden, available at: <https://mluk.brandenburg.de/Steckbriefe-BB-Boeden/SB-5-3-Braunerde-Fahlerde.pdf>, last access: 31 January 2020, 2005 (in German).
- Montelius, O.: Om tidsbestämning inom bronzeåldern med särskildt afseende på Skandinavien, in: *Kungl. Vitterhets historie och antikvitets akademis handlingar*, 30, Akademien Förlag, Stockholm, Sweden, 1885 (in Swedish).
- Murray, A. S. and Wintle, A. G.: The single aliquot regenerative dose protocol: potential for improvements in reliability, *Radiat. Meas.*, 37, 377–381, 2003.
- Nagel, D., Hermsdorf, N., Lippstreu, L., and Martiklos, G.: Geologische Übersichtskarte 1:200 000, Bundesanstalt für Geowissenschaften und Rohstoffe (BGR), Hannover, Blatt: CC 3134 Wittenberge, 2003 (in German).
- Naturalearthdata: Internal administrative boundaries, available at: <https://www.naturalearthdata.com/downloads/10m-cultural-vectors/>, last access: 21 April 2020.
- Offenedaten: Brandenburg Landkreise, available at: <https://offenedaten.de/dataset/landkreise-brandenburg>, last access: 21 April 2020.
- Pluckhahn, T. J., Hodson, A. D., Rink, W. J., Thomson, V. D., Hendricks, R. R., Doran, G., Farr, G., Cherkinsky, A., and Norman, S. P.: Radiocarbon and Luminescence Age Determinations on Mounds at Crystal River and Roberts Island, Florida, USA, *Geoarchaeology*, 30, 238–260, 2015.
- Porat, N., Duller, G. A. T., Roberts, H. M., Piasetzky, E., and Finkelshteyn, I.: OSL dating in multi-strata Tel: Megiddo (Israel) as a case study, *Quat. Geochronol.*, 10, 359–366, 2012.
- Prescott, J. R. and Hutton, J. T.: Cosmic ray distributions to dose rates for luminescence and ESR dating: large depths and long-term variations, *Radiat. Meas.*, 23, 497–500, 1994.
- Reimann, T., Naumann, M., Tsukamoto, S., and Frechen, M.: Luminescence dating of coastal sediments from the Baltic Sea coastal barrier-spit Darss-Zingst, NE Germany, *Geomorphology*, 122, 264–273, 2010.
- Reimann, T., Lindhorst, S., Thomas, K. J., Murray, A. S., and Frechen, M.: OSL dating of mixed coastal sediment (Sylt, German Bight, North Sea), *Quat. Geochronol.*, 11, 52–67, 2012.
- Reimann, T., Román-Sánchez, A., Vanwalleghem, T., and Wallinga, J.: Getting a grip on soil reworking—Single-grain feldspar luminescence as a novel tool to quantify soil reworking rates, *Quat. Geochronol.*, 42, 1–14, 2017.
- Saye, S. E. and Pye, K.: Variations in chemical composition and particle size of dune sediments along the west coast of Jutland, Denmark, *Sediment. Geol.*, 183, 217–242, 2006.
- Schoeneberger, P. J., Wysocki, D. A., and Benham, E. C.: Field book for describing and sampling soils, Version 3.0., Natural Resources Conservation Service, National Soil Survey Center, Lincoln, NE, USA, 2012.
- Schulte, L. and Wahnschaffe, F.: Geognostisch Agronomische Karte 1:25.000, Königliche Preussische Geologische Landesanstalt, Berlin, Blatt: 2837 Bäk (1900–1901), 1905.
- van der Meij, W. M., Reimann, T., Vornehm, V. K., Temme, A. J. A. M., Wallinga, J., van Beek, R., and Sommer, M.: Reconstructing rates and patterns of colluvial soil redistribution in agrarian (hummocky) landscapes, *Earth Surf. Proc. Land.*, 44, 2408–2422, 2019.
- Wüstemann, H.: Zur Sozialstruktur im Seddiner Kulturgebiet, *Z. Archäol.*, 8, 67–107, 1974 (in German).